Synthesis of site-specific antibody-drug conjugates using unnatural amino acids

Jun Y. Axup[a,b], Krishna M. Bajjuri[c], Melissa Ritland[d], Benjamin M. Hutchins[a,b], Chan Hyuk Kim[a,b], Stephanie A. Kazane[a,b], Rajkumar Halder[a,b], Jane S. Forsyth[d], Antonio F. Santidrian[d], Karin Stafin[d], Yingchun Lu[e], Hon Tran[e], Aaron J. Seller[e], Sandra L. Biroc[e], Aga Szydlik[e], Jason K. Pinkstaff[e], Feng Tian[e], Subhash C. Sinha[c], Brunhilde Felding-Habermann[d], Vaughn V. Smider[c,1], and Peter G. Schultz[a,b,1]

[a]Department of Chemistry, [c]Department of Molecular Biology, [d]Department of Molecular and Experimental Medicine, and [b]The Skaggs Institute for Chemical Biology, The Scripps Research Institute, La Jolla, CA 92037; and [e]Ambrx, Inc., La Jolla, CA 92037

Contributed by Peter G. Schultz, July 20, 2012 (sent for review January 27, 2012)

Antibody-drug conjugates (ADCs) allow selective targeting of cytotoxic drugs to cancer cells presenting tumor-associated surface markers, thereby minimizing systemic toxicity. Traditionally, the drug is conjugated nonselectively to cysteine or lysine residues in the antibody. However, these strategies often lead to heterogeneous products, which make optimization of the biological, physical, and pharmacological properties of an ADC challenging. Here we demonstrate the use of genetically encoded unnatural amino acids with orthogonal chemical reactivity to synthesize homogeneous ADCs with precise control of conjugation site and stoichiometry. *p*-Acetylphenylalanine was site-specifically incorporated into an anti-Her2 antibody Fab fragment and full-length IgG in *Escherichia coli* and mammalian cells, respectively. The mutant protein was selectively and efficiently conjugated to an auristatin derivative through a stable oxime linkage. The resulting conjugates demonstrated excellent pharmacokinetics, potent in vitro cytotoxic activity against Her2$^+$ cancer cells, and complete tumor regression in rodent xenograft treatment models. The synthesis and characterization of homogeneous ADCs with medicinal chemistry-like control over macromolecular structure should facilitate the optimization of ADCs for a host of therapeutic uses.

breast cancer | protein conjugation

A major challenge in the development of new drugs is the ability to selectively modulate a specific target in the tissue of interest while minimizing undesirable systemic side effects. In the past decade, antibody-drug conjugates (ADC) have shown considerable promise as anticancer agents by preferentially targeting cytotoxic drugs to cells presenting tumor-associated antigens (1–4). It is hypothesized that the ADCs are endocytosed after binding cell-surface antigens and the antibody molecule is degraded in the lysosome, releasing the cytotoxic drug into the cytosol (5, 6). Antibody-drug conjugates have had significant achievements as well as notable failures in the clinic. The first Food and Drug Administration-approved ADC, gemtuzumab ozogamicin (Mylotarg; Wyeth/Pfizer), was a conjugate of the DNA cleaving agent calicheamicin to an anti-CD33 antibody for the treatment of acute myelogenous leukemia (7). Despite early encouraging clinical activity and fast-track approval, Mylotarg was removed from the market because of toxicity and lack of efficacy in larger trials (8). More recently, however, brentuximab vedotin (Adcetris/SGN-35; Seattle Genetics), an anti-CD30 auristatin conjugate, became the first drug approved for Hodgkin's lymphoma since 1977 (9, 10), and there are many more ADCs in development (11–15). Although the approval of Adcetris shows the potential of ADCs to impact major unmet needs in oncology, the withdrawal of Mylotarg shows that further work is necessary to optimize this new class of drugs.

In contrast to small molecules, in which chemically defined structures are synthesized in an attempt to improve drug properties, the most widely used technologies for constructing antibody-drug conjugates rely on nonspecific electrophilic modification of cysteine or lysine residues. There is limited stoichiometric control because of the large number of disulfide bonds and lysine residues in antibody molecules, which leads to a typical distribution of zero to eight toxins per antibody (16, 17). In addition, coupling occurs at many different sites leading to a heterogeneous mixture of ADCs, the components of which likely have distinct affinities, stabilities, pharmacokinetics, efficacies, and safety profiles. Genentech reported a site-specific ADC (Thiomab) that was synthesized by introducing an additional cysteine into antibodies (18, 19). Thiomab showed similar efficacy to randomly labeled ADCs despite having fewer (only two) drugs per antibody, but had an improved therapeutic index and better pharmacokinetics in rodents. These results support the notion that precise chemical control over the site and stoichiometry of conjugates can lead to improved therapeutics. However, this methodology has not been generally adopted, likely in part because of challenges in scalability, which involves disulfide bond reduction and reoxidization steps, and the instability of maleimide-thiol conjugates (20).

Here we report the synthesis of chemically defined ADCs in which the site and stoichiometry of conjugation are controlled using genetically encoded unnatural amino acids with orthogonal chemical reactivity relative to the canonical 20 amino acids. This approach produces homogeneous molecular entities, rather than mixtures, and allows for medicinal chemistry-like optimization of physical properties, efficacy, pharmacokinetics, and safety profiles. An orthogonal amber suppressor tRNA/aminoacyl-tRNA synthetase (aaRS) pair is used to site-specifically incorporate *p*-acetylphenylalanine (pAcPhe) in response to an amber nonsense codon into antibodies recombinantly expressed in either bacterial or mammalian cells (21–24). The keto group of pAcPhe can be selectively coupled to an alkoxy-amine derivatized drug of interest to form a stable oxime bond in excellent yield (25–27). To illustrate this concept, a C-terminal alkoxy-amine auristatin derivative was conjugated to trastuzumab (Herceptin, anti-Her2) mutants containing pAcPhe at one of several positions in the antibody constant regions. The resulting ADCs showed excellent efficacy and pharmacokinetics in an in vivo rodent xenograft model against mammary fat pad tumors induced by Her2-transduced MDA-MB-435 human breast cancer cells.

Author contributions: J.Y.A., B.M.H., V.V.S., and P.G.S. designed research; J.Y.A., K.M.B., M.R., B.M.H., J.S.F., A.F.S., S.L.B., and A.S. performed research; J.Y.A., K.M.B., B.M.H., C.H.K., S.A.K., R.H., J.S.F., K.S., Y.L., H.T., A.J.S., and F.T. contributed new reagents/analytic tools; J.Y.A., K.M.B., M.R., B.M.H., C.H.K., S.A.K., R.H., A.F.S., S.L.B., A.S., J.K.P., F.T., S.C.S., B.F.-H., V.V.S., and P.G.S. analyzed data; and J.Y.A., V.V.S., and P.G.S. wrote the paper.

The authors declare no conflict of interest.

[1]To whom correspondence may be addressed. E-mail: vvsmider@scripps.edu or schultz@scripps.edu.

This article contains supporting information online at www.pnas.org/lookup/suppl/doi:10.1073/pnas.1211023109/-/DCSupplemental.

BIOCHEMISTRY

Results and Discussion

Design of an Anti-Her2 ADC. Trastuzumab (anti-Her2 antibody) strongly binds Her2 (ErbB2), a member of the epidermal growth factor receptor family of receptor tyrosine kinases that is overexpressed in 25–30% of breast cancers (28). Furthermore, the Her2 receptor shows little normal tissue expression and is known to internalize readily, making it a good candidate for ADC targeting. Indeed, Genentech has nonspecifically conjugated maytansine (DM1) to trastuzumab to produce an ADC that has shown excellent efficacy in preclinical and phase I and II clinical trials (11, 29).

The most commonly used toxins for ADCs in clinical development are maytansine (11–13), calicheamicin (7, 14), and auristatin (10, 15). We chose to use auristatin, a highly potent tubulin inhibitor, because it is well characterized and can be modified for facile coupling to an antibody (10, 30). Although the first generation of auristatin-linker conjugates were coupled to the N terminus of the peptide and contained a cathepsin B protease cleavage site, Doronina et al. synthesized C-terminally linked derivatives that were reported to be more cytotoxic and have improved pharmacological profiles (30). Furthermore, Oflazoglu et al. have demonstrated that in some cases ADCs synthesized with noncleavable linkers are as potent as those containing cleavable linkers (31), presumably because of degradation of the ADC in the lysosome and release of drug. Therefore, we first chose to investigate ADCs containing a noncleavable linker (nAF) coupled to the C terminus of auristatin F (AF) (Fig. 1*A* and Scheme S1). The linker contains two ethylene glycol moieties modified with a terminal alkoxy-amine group to improve solubility and minimize export of the more hydrophilic derivatized analogs by drug pumps (32).

Preparation of Anti-Her2–Auristatin Conjugates. We generated auristatin conjugates of both the Fab fragment and the full-length IgG1 of trastuzumab to compare their in vitro activities. To site-specifically incorporate pAcPhe into the anti-Her2 Fab fragment, an orthogonal amber suppressor tRNA/aaRS pair, derived from the corresponding tyrosyl *Methanococcus jannaschii* pair and evolved to selectively incorporate pAcPhe (21–23), was coexpressed separately with anti-Her2 Fab genes containing a TAG

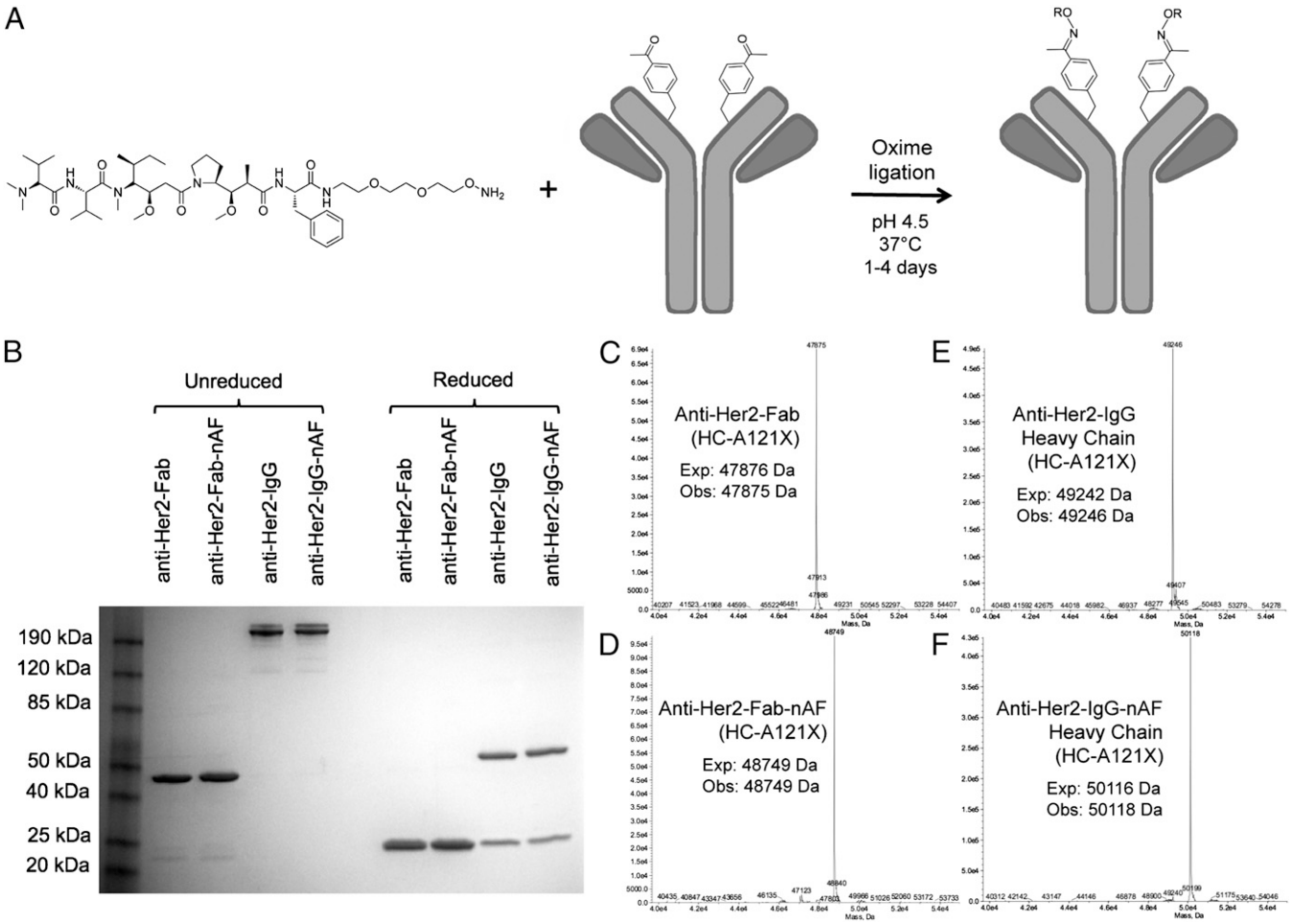

Fig. 1. Site-specific conjugation of alkoxy-amine–derivatized auristatin to anti-Her2 Fab and IgG with pAcPhe. (*A*) The noncleavable auristatin derivatized with a terminal alkoxy-amine is coupled by oxime ligation to antibodies through pAcPhe residues. (*B*) SDS/PAGE gel of anti–Her2-Fab (HC-A121X) and anti–Her2-IgG (HC-A121X) before and after coupling to auristatin. The unreduced Fab migrates at ~48 kDa and the reduced (50 mM DTT) Fab migrates as a single band at ~24 kDa. The IgG includes natural heterogeneous *N*-linked glycosylation; the reduced light chain is ~24 kDa and heavy chain is ~55 kDa (includes glycan). The 4–12% Tris-Glycine gel (Invitrogen) has Benchmark prestained protein ladder in the first lane and was stained with Coomassie. (*C–F*) ESI-MS of Fab (HC-A121X) and IgG (HC-A121X) before and after conjugation to auristatin. Fab spectra (*C* and *D*) correspond to the fully intact fragment, but IgG spectra (*E* and *F*) show only the heavy chain after deglycosylation with PNGase and reduction with 10 mM DTT. All masses are as expected with a ~874-Da difference between the conjugated and unconjugated heavy chains, corresponding to conjugation of one noncleavable auristatin per Fab or full-length heavy chain. No unreacted antibody was observed by SDS/PAGE or ESI-MS, suggesting >95% coupling efficiency.

codon at residue K169 (LC-K169X) or S202 (LC-S202X) on the light chain, or A121 (HC-A121X) on the heavy chain (Fig. S1*A*) (25, 26). These sites were chosen on the basis of their surface accessibility and previously demonstrated high expression yields and high coupling efficiencies (18, 26). The yields of all of these mutants were ~2 mg/L when grown in shake flasks and > 400 mg/L in high-density fermentors after periplasmic lysis and protein G purification, which is similar to the yield of wild-type Fab expressed and purified under the same conditions. The mutant anti-Her2 Fabs resolved into bands of ~48 kDa under nonreducing conditions and ~24 kDa after treatment with 10 mM DTT, when analyzed by gel electrophoresis (SDS/PAGE) (Fig. 1*B* and Fig. S1*B*). Electrospray-ionization mass spectrometry (ESI-MS) confirmed the expected molecular masses of the pAcPhe mutants (Fig. 1*C* and Fig. S2). The mutants bound the ErbB2 extracellular domain (Fc fusion; R&D Systems) with an affinity indistinguishable from the wild-type Fab, as determined by ELISA, with half-maximal binding (IC_{50}) of ~1 nM (Fig. S3).

An amber codon was substituted in the full-length anti-Her2 IgG1 gene at heavy-chain residue A121 (HC-A121X). The pAcPhe-containing antibody was recombinantly produced in suspension Chinese hamster ovary (CHO-K1) cells, in which an orthogonal *Escherichia coli* tyrosyl-derived tRNA/aaRS pair (24) that incorporates pAcPhe was first stably integrated into the genome using selectable markers. Next, the light chain and mutant heavy chain (HC-A121X) genes for the IgG were stably incorporated into the tRNA/aaRS-expressing CHO cell line. Stable pools yielded ~20 mg/L of the pAcPhe mutant antibody and stable clones produced over 300 mg/L. Folded IgG was collected from media and purified by protein G-affinity chromatography. The mutant anti–Her2-IgG was characterized by nonreducing SDS/PAGE (Fig. 1*B*) and showed a band at ~200 kDa. Reducing conditions (50 mM DTT) revealed a light-chain band at ~24 kDa and heavy-chain band at ~55 kDa, which includes *N*-linked glycosylation in the Fc region. To determine the molecular mass, the sample was treated with PNGase F (PROzyme) at 37 °C for >4 h to remove the glycans, followed by reduction with 10 mM DTT. ESI-MS analysis revealed a mass of 49,246 Da, corresponding to the trastuzumab heavy chain with pAcPhe replacing an alanine (Fig. 1*E*). The ELISA binding data for the mutant IgG was similar to that of Herceptin (IC_{50} of ~0.3 nM) (Fig. S3).

AF was synthesized as previously reported (30). The noncleavable ethylene glycol linker derivatized with an alkoxy-amine was synthesized, as previously described (33), and attached to the C terminus of AF (*SI Materials and Methods*). The pAcPhe-containing anti-Her2 Fab (100 μM) was coupled to the alkoxy-amine linker-derivatized AF (3 mM) in 100 mM ammonium acetate buffer, pH 4.5, at 37 °C for 16–48 h, followed by washing in an Amicon 10,000 molecular weight cutoff (MWCO) concentrator to remove excess drug-linker. Analysis by ESI-MS revealed that the Fab-drug conjugate had a mass 874 Da larger than the unconjugated Fab mutant, which corresponds to the mass of one nAF per Fab (Fig. 1*D* and Fig. S2). Under these conditions, no unconjugated Fab or degradation products were observed by SDS/PAGE or ESI-MS, indicating a >95% coupling efficiency. Conjugation reactions with the full-length IgG were carried out with 66.7 μM antibody and 1.3 mM auristatin-linker for 4 d in the same buffer. Anti–Her2-IgG-nAF was analyzed by ESI-MS after being treated with PNGase and DTT (Fig. 1*F*), which again revealed a mass difference of 872 Da between the unconjugated (49,246 Da) and drug-conjugated heavy chain (50,118 Da). Unreacted anti–Her2-IgG heavy chain or degradation products were undetectable by SDS/PAGE or ESI-MS, indicating an overall yield of >95% for conjugation of two auristatin derivatives per IgG. Thus, homogeneous products of Fab with one toxin and IgG with two toxins were produced by means of genetically encoded unnatural amino acids.

In Vitro Cytotoxicity. Anti–Her2-auristatin conjugates were tested on Her2-expressing breast cancer cells for cytotoxicity (MDA-MB-435 cells transduced with Her2, and SK-BR-3 cells), and $Her2^-$ cells (MDA-MB-435) for selectivity. MDA-MB-435/$Her2^+$ cells were generated by stable transduction of triple negative MDA-MB-435 cells with Her2 using a lentiviral vector that contains the full Her2 transmembrane receptor gene (26), providing an isogenic comparison cell line to the original $Her2^-$ MDA-MB-435 cell line (34–36). Anti–Her2-IgG with two nAFs conjugated at HC-A121X kills MDA-MB-435/$Her2^+$ cells with a EC_{50} of 0.37 ± 0.38 nM (mean ± SD), but does not kill MDA-MB-435/$Her2^-$ cells (EC_{50} >200 nM) (Fig. 2 *A* and *B*). The unconjugated auristatin-linker derivative kills both $Her2^+$ and $Her2^-$ MDA-MB-435 cells with an EC_{50} ~1 nM (1.5 ± 1.7 nM and 0.92 ± 2.4 nM, respectively). The cytotoxicity of the auristatin-linker is similar

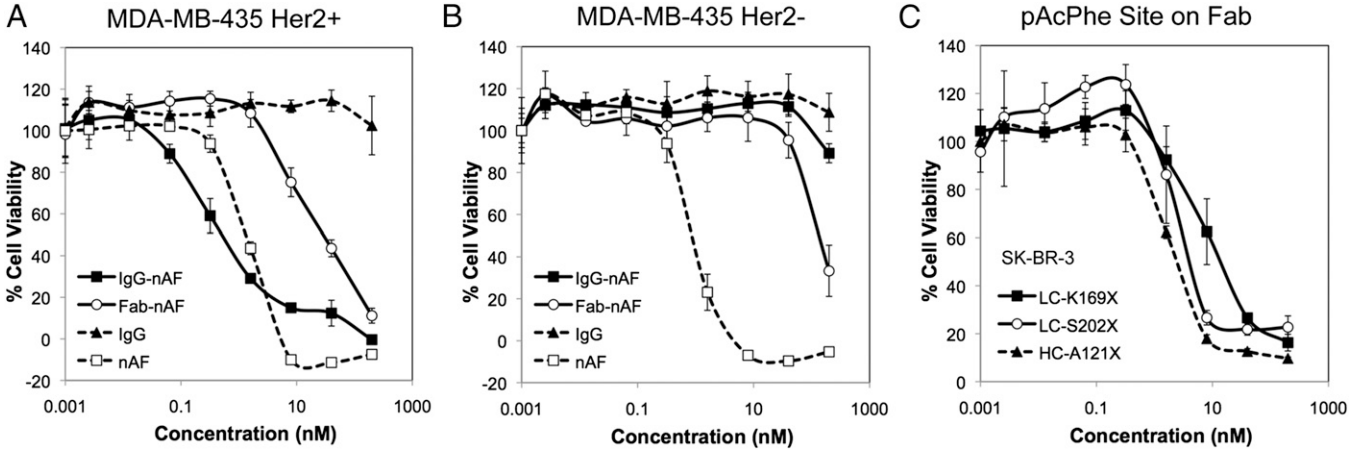

Fig. 2. In vitro cytotoxicity assays. (*A*) Anti–Her2-IgG(HC-A121X)-nAF (EC_{50} 0.37 ± 0.38 nM) is more cytotoxic than the unconjugated auristatin-linker (EC_{50} 1.5 ± 1.7 nM) and almost 100-times more cytotoxic than Fab(LC-K169X)-nAF (EC_{50} 21.3 ± 13.7 nM) on MDA-MB-435/$Her2^+$ cells. (*B*) IgG(HC-A121X)-nAF has little effect on MDA-MB-435/$Her2^-$ cells but the Fab-nAF is cytotoxic at >40 nM. The EC_{50} of the auristatin-linker alone on MDA-MB-435/Her^- cells is 0.92 ± 2.4 nM. (*C*) The cytotoxicity of nAF conjugated to sites LC-S202X (EC_{50} 2.1 ± 2.8 nM) and HC-A121X (EC_{50} 1.8 ± 0.33 nM) on the Fab were slightly greater than the cytotoxicity of Fab(LC-K169X)-nAF (EC_{50} 8.3 ± 3.4 nM) on SK-BR-3 cells. Percent viability is normalized between no compound and 5 μM taxol controls. Error bars represent SD of three replicates.

to that of IgG-nAF conjugate (which has two auristatins per molecule), despite distinct mechanisms of cellular uptake (passive diffusion and receptor internalization, respectively). These results indicate that active drug is being efficiently released, presumably because of lysosomal degradation of the ADC. The anti–Her2-Fab (LC-K169X)-nAF (EC_{50} 21.3 ± 13.7 nM), which only has one drug per Fab fragment, is ∼100-times less cytotoxic than the IgG-nAF (two drugs per IgG) on MDA-MB-435/$Her2^+$ cells. This difference is likely due to increased binding and internalization efficiency of the full-length antibody relative to the Fab fragment. Fab-nAF also showed some nonspecific cytotoxicity on MDA-MB-435/$Her2^-$ cells at high concentrations (>40 nM).

Previous studies have shown that the site of conjugation is important for binding and activity of antibody conjugates for certain applications (25, 37). Three sites on the Fab (LC-K169X, LC-S202X, HC-A121X) were evaluated for activity on SK-BR-3 cells. The HC-A121X ADC showed similar cytotoxity (EC_{50} 1.8 ± 0.33 nM) to the LC-S202X ADC (EC_{50} 2.1 ± 2.8 nM), which was slightly better than the LC-K169X ADC (EC_{50} 8.3 ± 3.4 nM) (Fig. 2*C*). All three residues were originally selected to be surface-exposed, in flexible loop regions, and directed away from the antigen binding sites (Fig. S1*A*) so as to minimize effects on binding and internalization. The similar efficacy of these molecules suggests that the site of conjugation does not significantly affect lysosomal release of the active drug.

We next tested the cytotoxicity of anti–Her2-IgG(HC-A121X)-nAF on three additional breast cancer cell lines: HCC-1954 ($Her2^+$), BT-474 ($Her2^+$), and MCF-7 ($Her2^-$) (Fig. S4). In general, the anti–Her2-IgG-nAF ADC showed similar EC_{50}s in SK-BR-3 cells (IgG-nAF EC_{50} 0.17 ± 0.05 nM; nAF EC_{50} 0.82 ± 0.54 nM), HCC-1954 cells (IgG-nAF EC_{50} 0.11 ± 0.22 nM; nAF EC_{50} 0.53 ± 0.27 nM), and BT-474 cells (IgG-nAF EC_{50} 0.35 ± 0.20 nM; nAF EC_{50} 2.0 ± 6.1 nM) (summarized in Table S1). This observation is consistent with previous literature for anti–Her2-IgG-DM1 ADCs (11). In the above three cell lines, the IgG-nAF had better cytotoxicity than unconjugated auristatin-linker, but the cytotoxicity of both are correlated in each cell line, suggesting the differences are more because of drug sensitivity than receptor levels or rate of internalization. MCF-7 is a $Her2^-$ cell line and showed no cytotoxicity with IgG-nAF (<40 nM), despite being susceptible to unconjugated nAF (EC_{50} 3.2 ± 2.0 nM).

A very important factor for the safety and efficacy of any ADC is its stability in serum. Therefore, the serum stability of anti–Her2-IgG-nAF was evaluated by incubating the conjugate with mouse serum for 3 d at 37 °C. The cytotoxity of the ADC was then compared with the corresponding untreated ADC, which was diluted into serum immediately before assay. The activities of the serum-incubated and untreated ADCs were identical on MDA-MB-435 $Her2^+$ and $Her2^-$ cells (Fig. S5). The result indicates no loss of activity because of ADC degradation, which is consistent with the known stability of oxime bonds and in contrast to site-dependent stability of maleimide-thiol conjugates (20).

Antitumor Activity in Vivo. Next, we examined the pharmacokinetics of anti–Her2-IgG(HC-A121X)-nAF in rodents because most ADCs have reduced half-lives compared with the native antibody (20, 38, 39). A single dose of 1 mg/kg anti–Her2-IgG-nAF in PBS was injected intravenously in five rats, and serum was collected at regular intervals for 14 d and analyzed by ELISA using antihuman κ-antibody. The serum concentration decreases for both IgG-nAF and the corresponding unconjugated mutant IgG at the same rate (Fig. 3*D*). Pharmacokinetic parameters were calculated by noncompartment modeling, and also did not show significant differences in clearance rates for IgG-nAF and IgG at 0.31 ± 0.03 mL/h/kg and 0.3 ± 0.11 mL/h/kg, respectively (Table S2). Thus, our site-specific ADCs have pharmacokinetics similar to the unconjugated antibody, and improved relative to many nonspecifically conjugated ADCs (38, 39). It is likely that

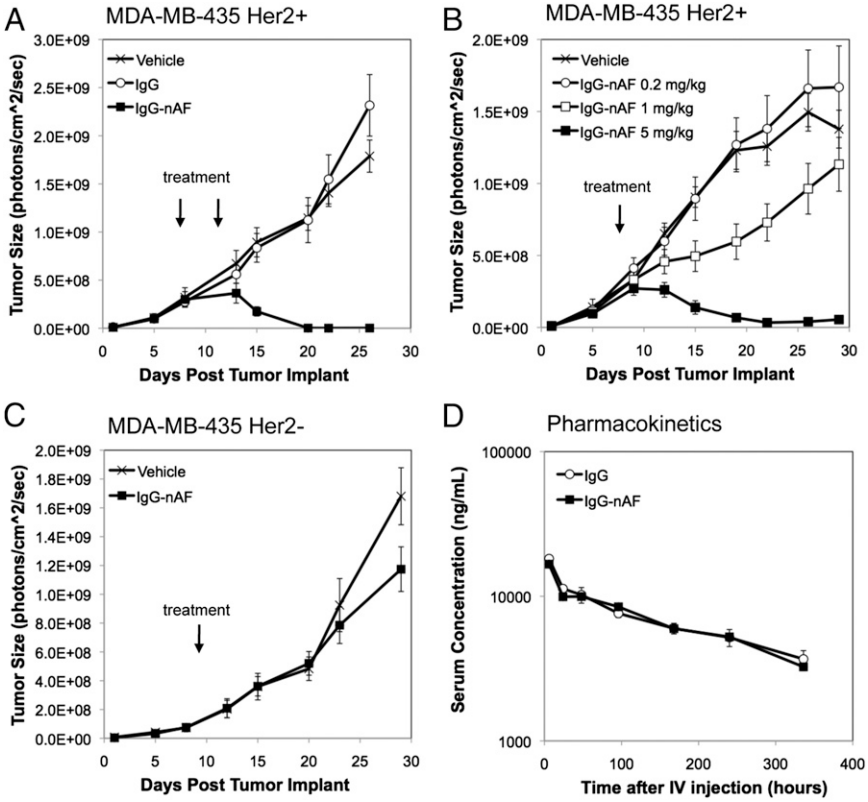

Fig. 3. In vivo efficacy and pharmacokinetics. (*A*) In vivo efficacy studies were performed with two 5 mg/kg i.v. doses of anti–Her2-IgG(HC-A121X)-nAF, anti–Her2-IgG alone, or DPBS against MDA-MB-435/$Her2^+$ tumors in C.B-1.7/SCID mice. Anti–Her2-IgG (HC-A121X)-nAF (■) shows reduction of MDA-MB-435/$Her2^+$ *F-luc* tumors 14 d after treatment (n = 8 mice/group; significant, P < 0.01). Tumors were implanted in the fourth mammary fat pad and sizes were monitored by longitudinal noninvasive bioluminescence imaging (IVIS 200; Caliper Life Science). (*B*) Dose effects were observed with a single injection of 5 mg/kg, 1 mg/kg, and 0.2 mg/kg (n = 8 mice/group). The 5-mg/kg group (■) had undetectable tumor after 14 d (significant, P < 0.01), the 1-mg/kg group (□) decreased the tumor, and 0.2 mg/kg (○) showed no difference from DPBS control. (*C*) MDA-MB-435/$Her2^-$ cells were treated in a similar manner with a single dose of 5 mg/kg anti–Her2-IgG-nAF. No regression of tumor was observed, and the growth curve was similar to that of DPBS control. (*D*) Pharmacokinetics study of serum concentration versus time of anti–Her2-IgG-nAF and anti–Her2-IgG in male Sprague–Dawley rats (n = 5 rats/group). Compound was injected at 1 mg/kg intravenously at time 0 and blood was collected at regular intervals for 14 d. Serum concentration was determined by capturing antibody with ErbB2 receptor protein and detecting with biotinylated anti-κ-antibody using 96-well Electro-ChemiLuminescent technology (Meso Scale Discovery). The IgG-nAF (■) was not different from unconjugated mutant IgG alone (○). Datapoints represent mean and error bars represent SEM.

nonspecific conjugates of hydrophobic drugs lead to a population of antibodies with reduced solubility.

Mouse xenograft studies were conducted with MDA-MB-435/Her2$^+$ cells injected in the fourth mammary fat pad of female C.B-17/SCID mice. The cells were stably transduced with Firefly luciferase (*F-luc*) so that tumor growth rates could be determined by longitudinal noninvasive bioluminescence imaging (IVIS 200; Caliper Life Science) (40–43). Eight days after mammary fat pad implantation of 2.5×10^5 tumor cells, the lesions emitted 10^8 photons per cm^2/s, and the mice were grouped into anti–Her2-IgG-nAF, unconjugated anti–Her2-IgG, and DPBS (Dulbecco's PBS) treatment arms ($n = 8$ each). IgG-nAF and IgG groups received two doses of 5 mg/kg on days 8 and 11, injected intravenously. Tumors treated with anti–Her2-IgG-nAF were barely detectable 14 d after treatment (significant, $P < 0.01$), whereas tumors in the unconjugated anti-Her2 IgG and DPBS groups continued to grow (Fig. 3*A* and Fig. S6). As SCID mice do not have adaptive immune systems, a significant treatment effect of unconjugated IgG by antibody-dependent cell-mediated cytotoxicity was not expected. Moreover, the similarity in response of the unconjugated IgG and DPBS groups indicates complement does not contribute significantly in this system.

Given the impressive response of tumors to the ADC, a second mouse in vivo study was conducted with a single dose of 5 mg/kg, 1 mg/kg, or 0.2 mg/kg (Fig. 3*B*). One 5-mg/kg dose cleared tumors within 14 d (significant, $P < 0.01$), indicating that this site-specific ADC with two drugs per antibody is highly efficacious. The 1-mg/kg dose decreased the tumor size but did not clear the tumors in <21 d and 0.2 mg/kg did not significantly differ from the PBS group. To test for in vivo selectivity for Her2-overexpressing tumors, MDA-MB-435/Her2$^-$ tumors were treated in a similar manner with a single dose of 5 mg/kg IgG-nAF and showed no significant difference from DPBS for 20 d after treatment (Fig. 3*C*). Throughout these studies the mice remained in good health and no weight loss or other overt toxicity was observed. H&E staining of liver and kidneys showed no obvious differences between treatment and control groups. Additionally, the groups did not differ in complete blood cell or metabolic profiles. Our results show that ADCs constructed with unnatural amino acids are highly potent and selective against Her2$^+$ tumors in vivo.

Conclusion

Genetically encoded unnatural amino acids with orthogonal chemical reactivity were used to create site-specific antibody-drug conjugates. The microtubule toxin AF was coupled to a single genetically encoded pAcPhe in an Fab and to two sites on an IgG, without coupling to any of the 20 canonical amino acid side chains. Antibodies containing pAcPhe were expressed as Fab fragments in *E. coli* and full-length IgG in mammalian cells, with yields comparable to the corresponding wild-type proteins. The oxime ligation reaction was optimized to afford high coupling efficiencies (>95%). The resulting conjugates showed selective in vitro cytotoxicity: anti–Her2-IgG-nAF had EC_{50} values in the 100–400 pM range on four Her2$^+$ cell lines. In xenograft models, MDA-MB-435/Her2$^+$ mammary fat pad tumors completely regressed to baseline levels in response to a single dose of 5 mg/kg anti–Her2-IgG-nAF; the ADC had no effect on Her2$^-$ MDA-MB-435 tumors. The pharmacokinetic profile of anti–Her2-IgG-nAF is similar to that of unconjugated IgG, and the ADC was stable in mouse serum. Thus, our anti–Her2-IgG-nAF conjugate is potent, selective, and has excellent serum half-life.

The ability to conjugate the drug component of an ADC selectively to a desired surface-exposed residue allows for structure-activity relationships to be evaluated in a manner similar to small molecule medicinal chemistry. Traditional protein conjugation chemistries via lysine or cysteine residues can generate mixtures of up to 10^6 species (16, 17) with different conjugation sites and stoichiometries, making optimization difficult. In contrast, conjugation to pAcPhe is chemically defined, efficient, and scalable, and the oxime linkage is highly stable, which should also reduce toxicity because of release of the free toxin in vivo. Indeed, although trastuzumab-DM1 has shown efficacy in humans, it has also induced irreversible axonal degradation in nonhuman primates, which may be because of either release of the free toxin or ADC species in the heterogeneous mixture with altered specificities or pharmacology (29). Moreover, maleimide conjugation has been shown to adversely affect the stability of ADCs (20). Nonspecific conjugation has also been shown to impact the selectivity of antibody-DNA conjugates in the applications of immuno-PCR and other diagnostics (37).

Control over the linkage and stoichiometry of drug coupling should also facilitate the generation and optimization of ADCs containing alternative payloads (e.g., kinase inhibitors, proteosome inhibitors, or DNA-modifying agents) or combinations of drugs. Drugs traditionally used for autoimmune, inflammatory, metabolic or other diseases could also have enhanced therapeutic indices and half-lives when coupled to the appropriate targeting antibody. In addition, it is likely that the site of conjugation will affect circulating or intracellular drug release when cleavable linkers are required to release unmodified drug (e.g., protease accessibility or disulfide stability). Finally, the same chemistry can be used to rapidly couple imaging agents to antibodies or fragments thereof, facilitating analysis of tumor localization/imaging with therapeutic treatment.

Materials and Methods

Expression of Antibodies with Unnatural Amino Acids. Expression of anti–Her2-Fab fragments was previously described (25) using pEVOL-pAcPhe (23). The mammalian expression system in suspension CHO cells involves stable incorporation of tRNA/aaRS pair and antibody genes.

Synthesis of Auristatin and Linkers. AF was synthesized as previously described (30). The noncleavable ethylene glycol linker was prepared as previously described (33) from commercial materials, and coupled to AF as described in *SI Materials and Methods*.

Conjugation. Oxime ligation between pAcPhe on the antibody and alkoxyamine-functionalized auristatin was carried out in 100 mM acetate buffer pH 4.5 with 100 μM (5 mg/mL) Fab and 3 mM AF (30-fold excess) for 1–2 d at 37 °C. IgG was conjugated at 66.7 μM (10 mg/mL) and 1.3 mM AF (20-fold excess) for 4 d at 37 °C. Buffer exchange with acetate buffer was done in an Amicon concentrator with 10,000 MWCO for Fabs and 30,000 MWCO for IgGs. Excess small molecule was removed by extensive washing through a 10,000 MWCO or 30,000 MWCO Amicon concentrator with PBS (pH 7.4).

ELISA. ELISA of anti-Her2 antibodies used human ErbB2 receptor Fc conjugate (R&D Systems) as capture antibody plated on high-binding 96-well plates (Nunc Maxisorp) and blocked with 3% milk (BioRad) in PBS with 0.1% Tween 20. Antibody and ADC were plated at dilutions from 0 to 40 nM in triplicate. Antibody concentrations were determined by BCA Protein Assay Kit (Pierce) using BSA as standards. After brief washing, goat antihuman κ-HRP conjugate (Sigma) was used at 1:1,000 dilution in blocking buffer. QuantaBlue fluorogenic peroxidase substrate (ThermoFisher) was used for detection and the plate was read on a spectrofluorometer (Molecular Devices) at excitation 325 nm and emission 420 nm.

In Vitro Cytotoxicity Assay. MDA-MB-435, SK-BR-3, HCC-1954, BT-474, and MCF-7 cell lines were obtained from ATCC. Cells were cultured and assayed in DMEM (Cellgro) with 10% (vol/vol) FBS (Gibco), 100 IU/mL penicillin, and 100 μg/mL streptomycin (Cellgro) for MDA-MB-435, SK-BR-3, and MCF-7. HCC-1954 cells were cultured in RPMI-1640 (Cellgro) and BT-474 cells were cultured in Hybri-care (ATCC), both supplemented with 10% FBS and PS. MDA-MB-435 Her2$^+$ cells were generated by transducing with lentivirus containing the wild-type Her2 receptor gene, as previously described (26). For the cytotoxicity assays, the cancer cell line of interest was plated in 96-well plates at ~1,000 cells in 90 μL per well in respective culture media and incubated overnight at 37 °C and 5% CO_2. Compounds were filtered (0.22 μm; Millipore) and 10× solutions were prepared in PBS as serial dilutions from 0 to 2 μM. Ten microliters from the 10× stocks were added to the 90 μL of cells in triplicate. Wells with PBS only and 5 μM taxol were used as 100% viability and 0% viability

BIOCHEMISTRY

controls, respectively. The wells on the outermost edges of the plate were filled with 200 μL of blank media and a metal plate cap was placed to prevent evaporation of sample wells. After 3 d of incubation, 20 μL of CellTiter-Blue (Promega) was added and incubated for 4 h before fluorescence was read at 560 nm excitation and 590 nm emission. Relative fluorescent units (RFU) were normalized to percent viability between no compound and taxol controls using the formula:

$$\%\text{Viability} = (\text{RFU} - \text{RFU}_{\text{taxol}})/(\text{RFU}_0 - \text{RFU}_{\text{taxol}}) \times 100\%. \quad [1]$$

Error bars in graphs represent SD of three replicates. EC_{50} values and EC_{50} SDs were determined using the Web applet at http://www.changbioscience.com/stat/ec50.html using the four parameter (log) setting.

Serum Stability Assay. Anti–Her2-IgG(HC-A121X)-nAF was incubated in mouse serum (BioChemed Services) at a 1:5 ratio for 3 d at 37 °C. Control sample was prepared by diluting IgG-nAF in mouse serum (1:5) immediately before the cytotoxicity assay.

Pharmacokinetic Study. Anti–Her2-IgG(HC-A121X)-nAF and unconjugated anti–Her2-IgG(HC-A121X) were administered to male, jugular vein cannulated, Sprague–Dawley rats (Charles River Laboratories) as a single bolus intravenous injection through the cannulus at time 0. Blood was collected at regular intervals for 14 d and processed to serum. The antibody and ADC were quantified in rat serum by capturing with human ErbB2-Fc (R&D Systems) and detecting with goat anti-human κ-biotinylated polyclonal antibody (SouthernBiotech) using 96-well ElectroChemiLuminescent technology (Meso Scale Discovery). The dynamic range for the assay is 10 ng/mL to 100,000 ng/mL. The serum concentrations for intravenously injected rat time points (from 6 to 336 h) were analyzed by noncompartment modeling using WinNonlin PK/PD Modeling and Analysis software (PharSight). All procedures were approved by the Ambrx, Inc. Animal Care and Use Committee and were performed according to national and international guidelines for the humane treatment of animals.

In Vivo Efficacy Model. All efficacy studies were conducted in 6- to 8-wk-old female C.B-17/SCID mice (Taconic Farms). The 2.5×10^5 MDA-MB-435/Her2+ F-luc cells in 30 μL were injected into the fourth mammary fat pad. Tumor cell growth was monitored biweekly by noninvasive bioluminescence imaging (IVIS 200; Caliper Life Science). Once an average lesion signal of 10^8 photons per cm^2/s was detected, mice were randomized into control or treatment groups. In the first study (Fig. 3*A*), mice were grouped ($n = 8$ each) on day 8 after tumor cell implantation and injected with 5 mg/kg anti–Her2-IgG-nAF, 5 mg/kg anti–Her2-IgG, or DPBS intravenously (100 μL). A second dose of 5 mg/kg IgG-nAF or IgG were administered on day 11. The dose titration study (Fig. 3*B*) involved a single dose of anti–Her2-IgG-nAF at 5 mg/kg, 1 mg/kg, 0.2 mg/kg, or DPBS control intravenously ($n = 8$ each) 8 d after tumor cell injection. In vivo selectivity (Fig. 3*C*) was evaluated by injecting MDA-MB-435/Her2$^-$ F-luc cells and a single treatment of 5 mg/kg anti–Her2-IgG-nAF or DPBS ($n = 5$ each) 9 d after tumor cell injection. After treatment, tumors continued to be monitored biweekly, and the mice were euthanized on day 29. Tumors were excised and weighed. H&E staining of liver and kidneys, hematological profile (Hemavet; Drew Scientific), and metabolite profiles (serum submission to RADIL, University of Missouri) were analyzed between treatment and control groups. *P* values and significance were analyzed by one-way ANOVA and Dunn's multiple comparison test. All procedures were approved by The Scripps Research Institute Animal Care and Use Committee and were performed according to national and international guidelines for the humane treatment of animals.

ACKNOWLEDGMENTS. This work was supported by American Cancer Society Grants ACS RSG-09-1601 (to V.V.S.), and R01GM062159 (to P.G.S.). This manuscript is number 21629 of The Scripps Research Institute.

1. Wu AM, Senter PD (2005) Arming antibodies: Prospects and challenges for immunoconjugates. *Nat Biotechnol* 23:1137–1146.
2. Polakis P (2005) Arming antibodies for cancer therapy. *Curr Opin Pharmacol* 5:382–387.
3. Lambert JM (2005) Drug-conjugated monoclonal antibodies for the treatment of cancer. *Curr Opin Pharmacol* 5:543–549.
4. Vater CA, Goldmacher VS (2010) Antibody-cytotoxic compound conjugates for oncology. *Macromolecular Anticancer Therapeutics* Part 4:331–369.
5. Kovtun YV, Goldmacher VS (2007) Cell killing by antibody-drug conjugates. *Cancer Lett* 255:232–240.
6. Okeley NM, et al. (2010) Intracellular activation of SGN-35, a potent anti-CD30 antibody-drug conjugate. *Clin Cancer Res* 16:888–897.
7. Hamann PR, et al. (2002) Gemtuzumab ozogamicin, a potent and selective anti-CD33 antibody-calicheamicin conjugate for treatment of acute myeloid leukemia. *Bioconjug Chem* 13:47–58.
8. Beck A, et al. (2010) The next generation of antibody-drug conjugates comes of age. *Discov Med* 10:329–339.
9. Francisco JA, et al. (2003) cAC10-vcMMAE, an anti-CD30-monomethyl auristatin E conjugate with potent and selective antitumor activity. *Blood* 102:1458–1465.
10. Doronina SO, et al. (2006) Enhanced activity of monomethylauristatin F through monoclonal antibody delivery: Effects of linker technology on efficacy and toxicity. *Bioconjug Chem* 17:114–124.
11. Lewis Phillips GD, et al. (2008) Targeting HER2-positive breast cancer with trastuzumab-DM1, an antibody-cytotoxic drug conjugate. *Cancer Res* 68:9280–9290.
12. Tolcher AW, et al. (2003) Cantuzumab mertansine, a maytansinoid immunoconjugate directed to the CanAg antigen: A phase I, pharmacokinetic, and biologic correlative study. *J Clin Oncol* 21:211–222.
13. Goff LW, et al. (2009) A phase II study of IMGN242 (huC242-DM4) in patients with CanAg-positive gastric or gastroesophageal (GE) junction cancer. *J Clin Oncol* 27:e15625.
14. DiJoseph JF, et al. (2004) Antibody-targeted chemotherapy with CMC-544: A CD22-targeted immunoconjugate of calicheamicin for the treatment of B-lymphoid malignancies. *Blood* 103:1807–1814.
15. Tse KF, et al. (2006) CR011, a fully human monoclonal antibody-auristatin E conjugate, for the treatment of melanoma. *Clin Cancer Res* 12:1373–1382.
16. Hamblett KJ, et al. (2004) Effects of drug loading on the antitumor activity of a monoclonal antibody drug conjugate. *Clin Cancer Res* 10:7063–7070.
17. Wang L, Amphlett G, Blättler WA, Lambert JM, Zhang W (2005) Structural characterization of the maytansinoid-monoclonal antibody immunoconjugate, huN901-DM1, by mass spectrometry. *Protein Sci* 14:2436–2446.
18. Junutula JR, et al. (2008) Site-specific conjugation of a cytotoxic drug to an antibody improves the therapeutic index. *Nat Biotechnol* 26:925–932.
19. Junutula JR, et al. (2010) Engineered thio-trastuzumab-DM1 conjugate with an improved therapeutic index to target human epidermal growth factor receptor 2-positive breast cancer. *Clin Cancer Res* 16:4769–4778.
20. Shen B-Q, et al. (2012) Conjugation site modulates the in vivo stability and therapeutic activity of antibody-drug conjugates. *Nat Biotechnol* 30:184–189.
21. Wang L, Brock A, Herberich B, Schultz PG (2001) Expanding the genetic code of *Escherichia coli*. *Science* 292:498–500.
22. Wang L, Zhang Z, Brock A, Schultz PG (2003) Addition of the keto functional group to the genetic code of *Escherichia coli*. *Proc Natl Acad Sci USA* 100:56–61.
23. Young TS, Ahmad I, Yin JA, Schultz PG (2010) An enhanced system for unnatural amino acid mutagenesis in *E. coli*. *J Mol Biol* 395:361–374.
24. Liu W, Brock A, Chen S, Chen S, Schultz PG (2007) Genetic incorporation of unnatural amino acids into proteins in mammalian cells. *Nat Methods* 4:239–244.
25. Hutchins BM, et al. (2011) Site-specific coupling and sterically controlled formation of multimeric antibody fab fragments with unnatural amino acids. *J Mol Biol* 406:595–603.
26. Hutchins BM, et al. (2011) Selective formation of covalent protein heterodimers with an unnatural amino acid. *Chem Biol* 18:299–303.
27. Dirksen A, Hackeng TM, Dawson PE (2006) Nucleophilic catalysis of oxime ligation. *Angew Chem Int Ed Engl* 45:7581–7584.
28. Ross JS, et al. (2009) The HER-2 receptor and breast cancer: Ten years of targeted anti-HER-2 therapy and personalized medicine. *Oncologist* 14:320–368.
29. Krop IE, et al. (2010) Phase I study of trastuzumab-DM1, an HER2 antibody-drug conjugate, given every 3 weeks to patients with HER2-positive metastatic breast cancer. *J Clin Oncol* 28:2698–2704.
30. Doronina SO, et al. (2008) Novel peptide linkers for highly potent antibody-auristatin conjugate. *Bioconjug Chem* 19:1960–1963.
31. Oflazoglu E, et al. (2008) Potent anticarcinoma activity of the humanized anti-CD70 antibody h1F6 conjugated to the tubulin inhibitor auristatin via an uncleavable linker. *Clin Cancer Res* 14:6171–6180.
32. Zhao RY, et al. (2011) Synthesis and evaluation of hydrophilic linkers for antibody-maytansinoid conjugates. *J Med Chem* 54:3606–3623.
33. Jones DS, et al. (2001) Synthesis of LJP 993, a multivalent conjugate of the N-terminal domain of β2GPI and suppression of an anti-β2GPI immune response. *Bioconjug Chem* 12:1012–1020.
34. Chambers AF (2009) MDA-MB-435 and M14 cell lines: Identical but not M14 melanoma? *Cancer Res* 69:5292–5293.
35. Hollestelle A, Schutte M (2009) Comment Re: MDA-MB-435 and M14 cell lines: Identical but not M14 Melanoma? *Cancer Res* 69:7893–7893.
36. Prat A, et al. (2010) Phenotypic and molecular characterization of the claudin-low intrinsic subtype of breast cancer. *Breast Cancer Res* 12:R68.
37. Kazane SA, et al. (2012) Site-specific DNA-antibody conjugates for specific and sensitive immuno-PCR. *Proc Natl Acad Sci USA* 109:3731–3736.
38. Alley SC, et al. (2009) The pharmacologic basis for antibody-auristatin conjugate activity. *J Pharmacol Exp Ther* 330:932–938.
39. Boswell CA, et al. (2011) Impact of drug conjugation on pharmacokinetics and tissue distribution of anti-STEAP1 antibody-drug conjugates in rats. *Bioconjug Chem* 22:1994–2004.
40. Gross S, Piwnica-Worms D (2005) Spying on cancer: Molecular imaging in vivo with genetically encoded reporters. *Cancer Cell* 7:5–15.
41. Klerk CPW, et al. (2007) Validity of bioluminescence measurements for noninvasive in vivo imaging of tumor load in small animals. *Biotechniques* 43(1, Suppl):7–13, 30.
42. O'Neill K, Lyons SK, Gallagher WM, Curran KM, Byrne AT (2010) Bioluminescent imaging: A critical tool in pre-clinical oncology research. *J Pathol* 220:317–327.
43. Staflin K, et al. (2010) Targeting activated integrin alphavbeta3 with patient-derived antibodies impacts late-stage multiorgan metastasis. *Clin Exp Metastasis* 27:217–231.